A general decoding strategy explains the relationship between behavior and correlated variability

Amy M. Ni*[1,2], Chengcheng Huang[1,2,3], Brent Doiron[2,3], and Marlene R. Cohen[1,2]

[1]Department of Neuroscience, University of Pittsburgh, Pittsburgh, PA 15260, USA
[2]Center for the Neural Basis of Cognition, Pittsburgh, PA 15260, USA
[3]Department of Mathematics, University of Pittsburgh, Pittsburgh, PA 15260, USA

*Correspondence: amn75@pitt.edu

ABSTRACT

Improvements in perception are frequently accompanied by decreases in shared variability in sensory cortex. This relationship remains a mystery from a neural coding perspective because overall changes in shared variability minimally affect optimal information coding. We hypothesize that this relationship arises because instead of using optimal strategies for decoding the specific stimuli at hand, observers prioritize *generality*: a single set of neuronal weights to decode any stimuli. We tested this hypothesis using a combination of multineuron recordings in the visual cortex of rhesus monkeys performing a visually demanding task and a cortical circuit model. Our experimental and theoretical results demonstrate that a general decoding strategy explains the inverse relationship between perceptual performance and shared variability. The performance of a general decoder depended more on the magnitude of shared variability than the performance of a specific decoder, and the animals' decoding strategy more closely matched decoders optimized for broad rather than narrow sets of visual stimuli. These results support the idea that observers use a general sensory information decoding strategy capable of decoding neuronal responses to the wide range of stimuli encountered in natural vision.

INTRODUCTION

Many studies have demonstrated that increases in perceptual performance correspond to decreases in a very simple measure of shared variability in a population of sensory neurons: the mean correlation between the responses of a pair of neurons to repeated presentations of the same stimulus (termed spike count or noise correlations, or r_{SC}; Cohen & Kohn, 2011; Nirenberg & Latham, 2003; Cohen & Maunsell, 2009; 2011; Gregoriou et al., 2014; Gu et al., 2011; Herrero et al., 2013; Luo & Maunsell, 2015; Mayo & Maunsell, 2016; Mitchell et al., 2009; Nandy et al., 2017; Ni et al., 2018; Ruff & Cohen, 2014a; 2014b; 2016; 2019; Verhoef & Maunsell, 2017; Yan et al., 2014; Zénon & Krauzlis, 2012). We recently found that the axis in neuronal population space that explains the most mean correlated variability explains virtually all of the choice-predictive signals in visual area V4 (Ni et al., 2018).

These observations comprise a paradox because changes in this simple measure should have a minimal effect on information coding. Recent theoretical work shows that neuronal population decoders that extract the maximum amount of sensory information for the specific task at hand can easily ignore correlated noise that is restricted to a small number of dimensions (Kafashan et al., 2021; Kanitscheider et al., 2015b; Moreno-Bote et al., 2014; Pitkow et al., 2015; Rumyantsev et al., 2020; for review, see Kohn et al., 2016). The mean correlated variability of population activity in visual cortex is restricted to very few dimensions, occupying a low-dimensional subset of the full neuronal population space (Ecker et al., 2014; Goris et al., 2014; Huang et al., 2019; Kanashiro et al., 2017; Lin et al., 2015; Rabinowitz et al., 2015; Semedo et al., 2019; Williamson et al., 2016). Decoders for the specific task at hand can ignore mean correlated variability because it does not corrupt the dimensions of neuronal population space that are most informative about the stimulus (Moreno-Bote et al., 2014).

We propose a hypothesis that reconciles the numerous experimental observations of an inverse relationship between performance and mean correlated variability and these seemingly contradictory theoretical predictions. The theoretical predictions are predicated on the assumption that observers (and their neuronal population decoding mechanisms) use a decoding strategy that maximizes the amount of information extracted for the specific task at hand. We hypothesize that instead, observers use a *general* decoding strategy: one set of neuronal population decoding weights to extract sensory information about any visual stimuli.

Stimuli in the visual environment vary in many task-irrelevant as well as relevant features. Our idea is that the dimensions of the neural code that are optimal for the general decoding of any stimuli might be very similar to the axes that account for the mean correlated variability, because mean correlated variability is well known to depend on all of the stimulus features for which the population of neurons is tuned (Cohen & Kohn, 2011). If observers used this kind of general decoding strategy, their perceptual performance might be inextricably linked to mean correlated variability (Ruff et al., 2018). This decoding mechanism would explain the much-observed relationship between perceptual performance and mean correlated variability.

Here, we report the results of an initial test of this hypothesis. We used a simple, well-studied behavioral task to test whether a more-general decoder (optimized for a broader range of stimulus values) better explained the relationship between behavior and mean correlated variability than a more-specific decoder (optimized for a narrower range of stimulus values). Specifically, we used a well-studied orientation change-detection task (Cohen & Maunsell, 2009) to test whether a general decoder for the full range of stimulus orientations better explained the

relationship between behavior and mean correlated variability than a specific decoder for the orientation change presented in the behavioral trial at hand.

This is an important initial test of the general decoder hypothesis because many of the studies that found that performance increased when mean correlated variability decreased used a change-detection task (Cohen & Maunsell, 2009; 2011; Herrero et al., 2013; Luo & Maunsell, 2015; Mayo & Maunsell, 2016; Nandy et al., 2017; Ni et al., 2018; Ruff & Cohen, 2016; 2019; Verhoef & Maunsell, 2017; Yan et al., 2014; Zénon & Krauzlis, 2012). This task has been studied frequently because it is a simple laboratory version of a real-life scenario: the observer must report that a stimulus changed, regardless of the magnitude of the change.

For this test, we used a combination of experiments and theory. We used multineuron recordings in two rhesus monkeys to directly compare the effects of modulating visual attention on the mean correlated variability of the neuronal population to the effects of attention on the monkeys' neuronal decoding strategy. We then used a cortical circuit model to compare the effects of attention on the monkeys' decoding strategy to the effects of attention on an ideal general decoder for all orientations.

Our combined electrophysiological and theoretical results support our general decoder hypothesis. They demonstrate that using a single set of neuronal weights to decode sensory neuron population responses to any stimulus change can explain the frequently observed relationship between performance and mean correlated variability.

RESULTS

A behavioral framework for studying the general decoder hypothesis

We designed a behavioral task for two rhesus monkeys that allowed us to test the hypothesis that the relationship between perceptual performance and correlated variability is better explained by a more-general decoding strategy. This test required two main components. First, we used an orientation change-detection task with multiple potential orientation changes (**Fig. 1a**; different aspects of these data were presented previously, Ni et al., 2018). This allowed us to analyze decoders optimized for narrower versus broader ranges of stimulus orientations. Two Gabor stimuli of the same orientation flashed on and off until, at a random time, the orientation of one of the stimuli changed. The changed orientation was randomly selected from five options (**Fig. 1b**). The monkey could not predict which orientation change was to be detected on any given trial and was rewarded for responding to any orientation change.

Second, we made a manipulation designed to create a larger dynamic range of perceptual performance. We manipulated visual attention within the task (**Fig. 1a**) using a classic Posner cueing paradigm (Posner, 1980). Cued trials were collected for all five change amounts and uncued trials were collected mainly for the median change amount (**Fig. 1b**). Our attention analyses focused on this median change amount, for which we had both cued and uncued trials.

Figure 1

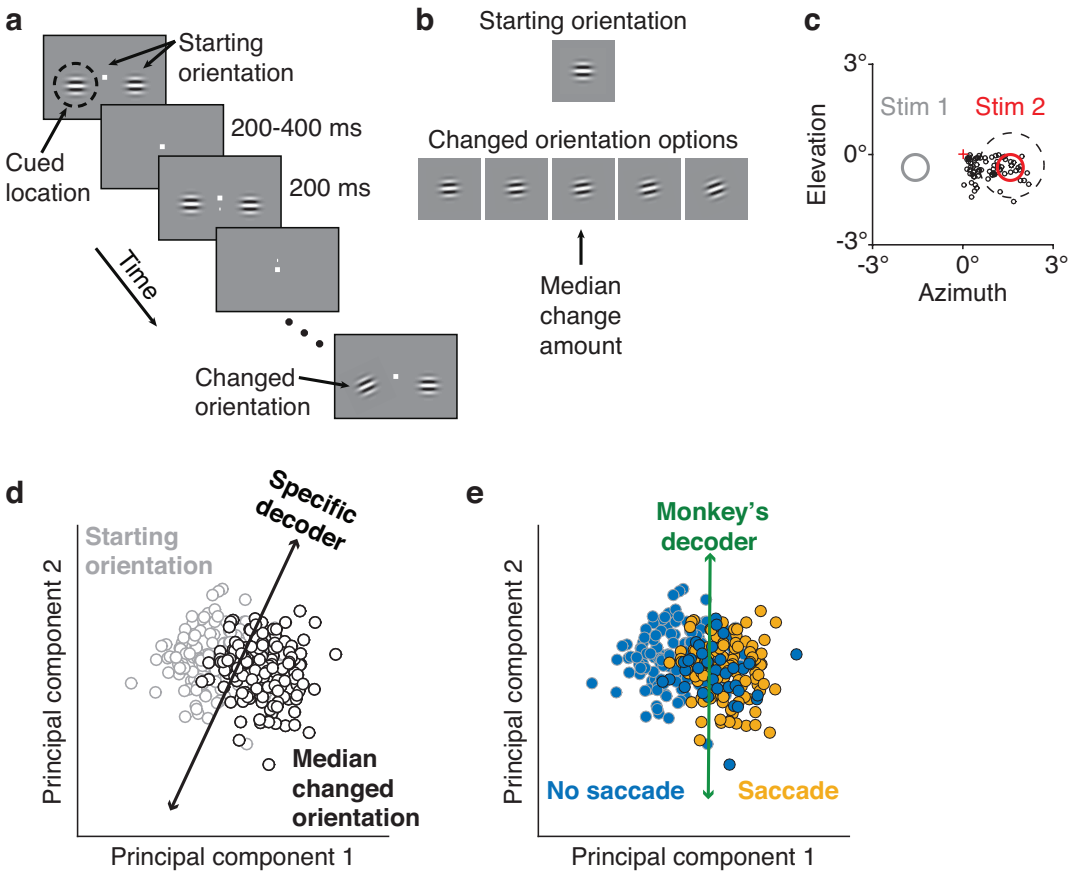

Figure 1. Electrophysiological data collection and decoders. (**a**) Orientation change-detection task with cued attention. After the monkey fixated the central spot, two Gabor stimuli

synchronously flashed on (200 ms) and off (randomized 200-400 ms period) at the starting orientation until, at a random time, the orientation of one stimulus changed. To manipulate attention, the monkey was cued in blocks of 125 trials as to which of the two stimuli would change in 80% of the trials in the block, with the change occurring at the uncued location in the other 20%. (**b**) A cued changed orientation was randomly assigned per trial from five potential orientations. An uncued changed orientation was randomly either the median (20 trials) or largest change amount (5 trials). To compare cued to uncued changes, median orientation change trials were analyzed. (**c**) The activity of a neuronal population in V4 was recorded simultaneously. Plotted for Monkey 1: the location of Stimulus 2 (red circle) relative to fixation (red cross) overlapped the receptive field (RF) centers of the recorded units (black circles). A representative RF size is illustrated (dashed circle). Only orientation changes at the RF location were analyzed. Stimulus 1 was located in the opposite hemifield (gray circle). (**d**) Schematic of the specific decoder, a linear classifier with leave-one-out cross-validation, which was trained to best differentiate the V4 neuronal population responses to the median changed orientation from the V4 responses to the starting orientation presented immediately before it (first and second principal components [PC] shown for illustrative purposes). (**e**) Schematic of the monkey's decoder, which was based on the same neuronal population responses as in (**d**) but was trained to best differentiate the V4 responses when the monkey made a saccade (indicating it detected an orientation change) from the V4 responses when the monkey did not choose to make a saccade.

For each monkey, we used a chronically implanted microelectrode array to record from a population of V4 neurons while the monkey performed the behavioral task (**Fig. 1c**). These electrophysiological recordings allowed us to measure the effects of attention on the mean correlated variability of the V4 population. They also allowed us to measure to the effects of attention on the performance of two linear decoders of the V4 population activity: a specific decoder (**Fig. 1d**) and the monkey's decoder (**Fig. 1e**).

We tasked both decoders with differentiating the V4 neuronal population responses to the median changed orientation from the V4 responses to the starting orientation presented immediately before it. We first estimated the neuronal decoding weights that best performed this specific task (**Fig. 1d**). Theoretical studies have found that mean correlated variability should not affect the performance of such an optimal linear decoder (Kafashan et al., 2021; Kanitscheider et al., 2015b; Moreno-Bote et al., 2014; Pitkow et al., 2015; Rumyantsev et al., 2020; reviewed by Kohn et al., 2016).

To compare the monkey's strategy to the performance of the specific decoder, we estimated the neuronal decoding weights that best predicted the monkey's pattern of choices on this same task (**Fig. 1e**). This allowed us to directly compare the performance of the monkey's decoder to that of the specific decoder on the same task. Using leave-one-out cross-validation, we calculated the ability of each decoder to correctly identify whether the left-out orientation was the median changed orientation or the starting orientation.

A mechanistic circuit model to test the general decoder hypothesis

Here, we describe a circuit model that we designed to allow us to compare the electrophysiological specific and monkey's decoders to modeled ideal specific and general decoders. For our electrophysiological dataset, the behavioral task was designed to allow us to compare the specific and monkey's decoders on a task with a range of orientation change amounts. To collect the necessary number of repetitions of behavioral trials per stimulus

condition (with the limited total number of behavioral trials collected per day), we limited the number of orientation changes to five (**Fig. 1b**). With our modeled dataset, we were able to compare the electrophysiological decoders to modeled ideal specific and general decoders. Because the ideal general decoder was based on a modeled dataset, we were able to calculate the responses of the network to the full range of stimulus orientations.

Our circuit model is an extension of our previously published excitatory/inhibitory cortical network model of attention (Huang et al., 2019). We improved this model to allow us to calculate the network's responses to the full range of stimulus orientations by extending the three-layer model of V1 and V4 neuronal populations (Huang et al., 2019; 2020) to mimic realistic orientation tuning and organization in the V1 layer (**Fig. 2a**).

This model is key to this initial test of the general decoder hypothesis because it allowed us test an ideal general decoder that used the same set of neuronal weights to estimate the full range of orientations (see **Methods**). Further, this specific model is key to our study because it is the only model (to our knowledge) that captures the effects of attention on correlated variability that have been frequently observed in electrophysiological data (Huang et al., 2019).

As the basis for our modeled specific and general decoders, we first mapped the *n*-dimensional neuronal activity of our model in response to the full range of orientations to a 2-dimensional space (a ring; **Fig. 2b & c**). The fluctuations of the neurons, mapped to the radial direction on the ring, were modeled as being more elongated in the unattended state (**Fig. 2b**) than in the attended state (**Fig. 2c**). We then calculated the effect of this attentional change on the performances of modeled ideal specific and general decoders, which we will compare to our electrophysiological results in the next section. The specific decoder used optimal neuronal weights (for *n* neurons in the population) based on the *n*-dimensional discrimination of two orientations (θ_1 and θ_2 in **Fig. 2b**). The general decoder was also tested on the discrimination of those same two orientations (θ_1 and θ_2 in **Fig. 2b**), but the neuronal weights of the general decoder were based on the neuronal population responses to all of the orientations in the ring (see **Methods** for details).

We note two more benefits of our model. The model more than captured our electrophysiologically recorded attentional changes in V4 firing rates (**Fig. 2d**), mean correlated variability (**Fig. 2e**), and covariance eigenspectrum (**Fig. 2f**). In fact, the model allowed us to test much larger modeled ranges of those values than those we recorded (**Fig. 2d-f**). We predict that the model, with its much wider range of mean correlated variability changes, will model stronger relationships to mean correlated variability than our electrophysiological data. Finally, our model will also allow us to test a much larger range of neuronal population sizes.

Figure 2

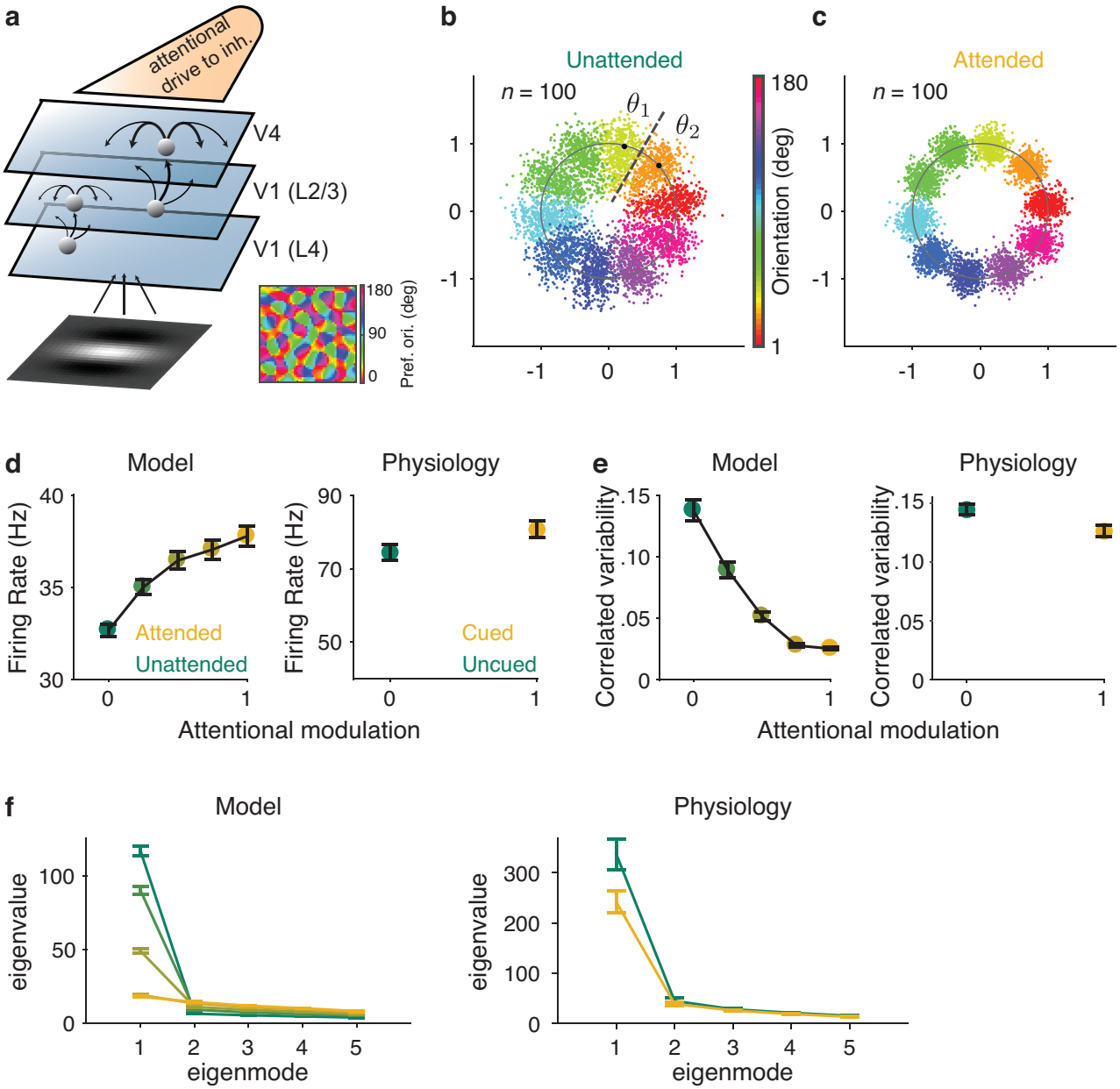

Figure 2. Mechanistic circuit model of attention effects. (**a**) Schematic of an excitatory and inhibitory neuronal network model of attention (Huang et al., 2019) that extends the three-layer, spatially ordered network to include the orientation tuning and organization of V1. The network models the hierarchical connectivity between layer 4 of V1, layers 2 and 3 of V1, and V4. In this model, attention depolarizes the inhibitory neurons in V4 and increases the feedforward projection strength from layers 2 and 3 of V1 to V4. (**b, c**) We mapped the *n*-dimensional neuronal activity of our model to a 2-dimensional space (a ring). Each dot represents the neuronal activity of the simulated population on a single trial and each color represents the trials for a given orientation. The fluctuations of the neurons are proportional to their firing rates and are mapped to the radial direction. These fluctuations are more elongated in the (**b**) unattended

state than in the (**c**) attended state. We then calculated the effects of these attentional changes on the performance of specific and general decoders (see **Methods**). (**d-f**) Comparisons of the modeled versus electrophysiologically recorded effects of attention on V4 population activity. (**d**) Firing rates of excitatory neurons increased, (**e**) mean correlated variability decreased, and (**f**) as illustrated with the first five largest eigenvalues of the shared component of the spike count covariance matrix from the V4 neurons, attention largely reduced the eigenvalue of the first mode. Attentional state denoted by marker color for the model (yellow: most attended; green: least attended) and electrophysiological data (yellow: cued; green: uncued). For the model: 30 samplings of $n = 50$ neurons. Monkey 1 data illustrated for the electrophysiological data: $n = 46$ days of recorded data. SEM error bars.

A general decoding strategy may clarify the role of mean correlated variability

First, we analyzed whether the relationship between attention, behavior, and mean correlated variability could be explained by a specific decoding strategy. This is an important first step because theoretical studies, which do not predict a relationship between mean correlated variability and performance, typically model decision-making as based on an optimal decoding strategy that maximizes the sensory information extracted from the neuronal population activity (Kafashan et al., 2021; Kanitscheider et al., 2015b; Moreno-Bote et al., 2014; Pitkow et al., 2015; Rumyantsev et al., 2020). A resolution to the apparent conflict between theoretical predictions and empirical results would be that perceptual performance is not based on a specific decoding strategy.

Indeed, we found that the effects of attention on the performance of the monkey's decoder did not match the effects of attention on the performance of the specific decoder (**Fig. 3a**). Manipulating attention affected the performance of each decoder differently: the performance of the specific decoder was little affected by attention, while that of the monkey's decoder was strongly affected by attention.

Second, we used our circuit model of attention to test whether a modeled ideal general decoder was a better match to the physiological monkey's decoder than a modeled ideal specific decoder. The model allowed us to generate a large dataset with an experimentally unfeasible number of trials per stimulus orientation for a full ring of stimulus orientations, in multiple attention conditions (**Fig. 2b & c**). The model also allowed us to test a much larger range of neuronal population sizes.

We found that the large effects of attention on the physiological monkey's decoder (**Fig. 3a**) were better matched by the similarly large effects of attention on the modeled general decoder (**Fig. 3b**) than by the small effects of attention on the modeled specific decoder (**Fig. 3b**). In other words, the monkey's decoding strategy was most qualitatively matched to the modeled general decoder.

The model allowed us to test a much larger range of population sizes than our electrophysiological recordings. We note that the effects of attention on the modeled general decoder (**Fig. 3b**) matched the effects of attention on the physiological monkey's decoder (**Fig. 3a**) in the neuronal population size range recorded in the physiological data. But we also observed that the difference in the attentional effects on the two modeled decoders decreased with larger population sizes (right plot of **Fig. 3b**). This is not noteworthy in and of itself because the attentional effects necessarily decreased as the decoders reached their information saturation points, as defined by the parameters of the modeled neurons. What we do want to note, however, is that the large attentional effects on the physiological monkey's decoders suggest that the

monkeys were not working in the optimal regime near the saturation point. Instead, the monkeys appear to have been working at an inner regime that allowed them to demonstrate large effects of attention on their performance.

Third, we tested the crux of our hypothesis: that a general decoding strategy underlies the frequently reported relationship between perceptual performance and mean correlated variability. This was our most critical test towards understanding the much debated role of mean correlated variability. It would be difficult to interpret a relationship between the performance of a decoder and mean correlated variability in isolation, because a correlation between these two factors could come about through an indirection relationship. But here, we tested the explicit hypothesis that the modeled general decoder would be more related to mean correlated variability than the modeled specific decoder, just as the physiological monkey's decoder would be more strongly related to mean correlated variability than the physiological specific decoder. Such a finding would indicate that a more-general decoding strategy better explained the relationship between behavior and mean correlated variability than a more-specific decoding strategy.

Indeed, we found that just as the performance of the physiological monkey's decoder was more strongly related to mean correlated variability than the performance of the physiological specific docoder (**Fig. 3c**), the performance of the modeled general decoder was more strongly related to mean correlated variability than the performance of the modeled specific decoder (**Fig. 3d**). As predicted, because we were able to test a much wider range of mean correlated variability values with the modeled neurons (**Fig. 2e**), we modeled much stronger relationships to correlated variability than observed with our physiological data (**Fig. 3c & d**). We observed that the correlation with specific decoder performance was significant with the modeled data but not with the physiological data. This is not surprising as we saw attentional effects, albeit small ones, on specific decoder performance with both the physiological and the modeled data (**Fig. 3a & b**). Even small attentional effects would result in a correlation between decoder performance and mean correlated variability with a large enough range of mean correlated variability values. As described above, our focus is not on whether the performance of any one decoder is significantly correlated with mean correlated variability, but on which decoder provides a better explanation of the frequently observed relationship between performance and mean correlated variability. Even with the wide range of mean correlated variability values tested with our model, the performance of the general decoder was more strongly related to mean correlated variability than the performance of the specific decoder.

Finally, while the circuit model allowed us to analyze an ideal general decoder for the full range of stimulus orientations in multiple attention conditions (**Fig. 2b & c**; a full ring of orientations in both unattended and attended conditions), as a sanity check, we used the physiological dataset (**Fig. 1b**; a limited set of five orientation change amounts in the cued condition only) to test whether more-general decoders were more related to the monkey's decoder than more-specific decoders. Would a decoder based on more stimulus orientations be more related to the monkey's decoder than a decoder based on fewer stimulus orientations?

For the physiological data, we again used linear decoders as illustrated in **Fig. 1d & e**, as the V4 neuronal population representations of the limited range of stimulus orientations tested in our behavioral task (**Fig. 1b**) were reasonably approximated by a line (**Fig. 3e**). First, for each monkey, we calculated the across-days Pearson's correlation between the performance of the monkey's decoder and the performance of a decoder based on a single orientation change amount (**Fig. 3f**, '1 ori'; see **Methods** for more details). Next, we calculated the across-days Pearson's correlation between the performance of the monkey's decoder and the performance of

decoders based on two, three, or four orientation change amounts (**Fig. 3f**, '2 oris' through '4 oris'). We found that the more general the decoder, the more its performance was correlated with that of the monkey's decoder.

Figure 3

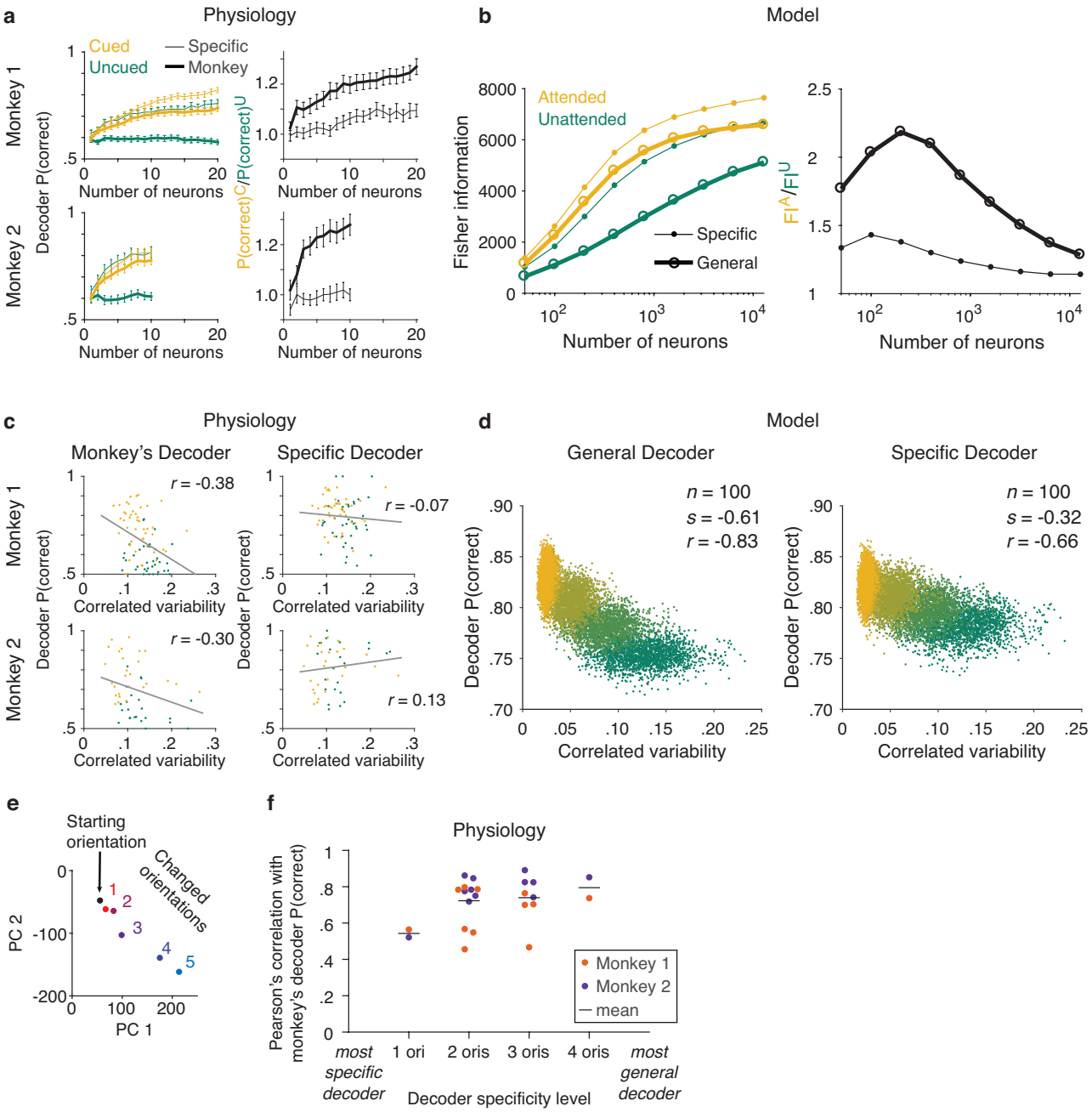

Figure 3. The monkey's decoding strategy was most closely matched by a general decoding strategy. (**a**) Physiological data for Monkey 1 and Monkey 2: the effect of attention on decoder performance was larger for the monkey's decoder than for the specific decoder. Left plots: decoder performance (*y*-axis; leave-one-out cross-validated proportion of trials in which the orientation was correctly identified: starting vs. median changed orientation) for each neuronal

population size (x-axis) is plotted for the specific (thin lines) and monkey's (thick lines) decoders in the cued (yellow) and uncued (green) attention conditions. Right plots: the ratio of the decoder performance in the cued versus uncued conditions is plotted for each neuronal population size. SEM error bars (Monkey 1: n = 46 days; Monkey 2: n = 28 days). (**b**) Modeled data: the effect of attention on decoder performance was larger for the general decoder than for the specific decoder. Left plot: the inverse of the variance of the estimation of theta (y-axis; equivalent to linear Fisher information for the specific decoder) for each neuronal population size (x-axis) is plotted for the specific decoder (small markers; **Eq. 1**, see **Methods**) and for the general decoder (large markers; **Eq. 3**, see **Methods**) in the attended (yellow) and unattended (green) conditions. Right plot: the ratio of Fisher information in the attended versus unattended conditions is plotted for each neuronal population size. (**c**) Physiological data for Monkey 1 and Monkey 2: the performance of the monkey's decoder was more related to mean correlated variability (left plots, gray lines of best fit; Monkey 1 Pearson's correlation coefficient: n = 86, or 44 days with two attention conditions plotted per day and two data points excluded – see **Methods**, r = -0.38, p = 5.9 x 10^{-4}; Monkey 2: n = 54, or 27 days with two attention conditions plotted per day, r = -0.30, p = 0.03) than the performance of the specific decoder (right plots; Monkey 1 Pearson's correlation coefficient: r = -0.07, p = 0.53; Monkey 2: r = 0.13, p = 0.36). For both monkeys, the correlation coefficients associated with the two decoders were significantly different from each other (Williams' procedure; Monkey 1: t = 3.7, p = 2.3 x 10^{-4}; Monkey 2: t = 3.2, p = 1.4 x 10^{-3}). (**d**) Modeled data: the performance of the general decoder was more related to mean correlated variability (left plot) than the performance of the specific decoder (right plot; number of neurons fixed at 100 and attentional state denoted by marker color, yellow: most attended, green: least attended). (**e**) An example plot of the first versus second PC of the V4 population responses to each of the six orientations presented in the session, to justify a linear decoding strategy for the more-general decoders (starting orientation illustrated in black, five changed orientations illustrated with a red-blue color gradient from smallest to largest). Though the brain may use nonlinear decoding methods, the neuronal population representations of the small range of orientations tested per day were reasonably approximated by a line; thus, linear methods were sufficient to capture decoder performance for the physiological dataset. (**f**) Physiological data for Monkey 1 (orange) and Monkey 2 (purple): the more general the decoder (x-axis; number of orientation changes used to determine the decoder weights, with the decoder that best differentiated the V4 responses to the starting orientation from those to one changed orientation on the far left, and the decoder that best differentiated V4 responses to the starting orientation from those to four different changed orientations on the far right), the more correlated its performance to the performance of the monkey's decoder (y-axis; the across-days Pearson's correlation between the performance of the monkey's decoder and the performance of the decoder specified by the x-axis). Mean across all points in a column illustrated by a black horizontal line (see **Methods** for n values).

DISCUSSION

Our results suggest that the relationship between behavior and mean correlated variability is explained by the hypothesis that observers use a general strategy that employs the same neuronal weights for decoding any stimulus change. The modeled general decoder better matched the attentional effects on the electrophysiological monkey's decoder and, most importantly, was more strongly related to mean correlated variability than the specific decoder. Further, based on our electrophysiological data, the more general the decoder (the more orientation change amounts used to determine the decoder weights) the more its performance was correlated with that of the monkey's decoder. Together, these results support the hypothesis that observers use a general decoding strategy in scenarios that require flexibility to changing stimulus conditions.

Our study also demonstrates the utility of combining electrophysiological and circuit modeling approaches to studying neural coding. Our model mimicked the correlated variability and effects of attention in our physiological data. Using a circuit model allowed us to perform a very large number of trials for a full range of different stimulus orientations in multiple attention conditions, allowing us to test the effects of attention on a true general decoder for orientation. The model also allowed us to test large neuronal population sizes (**Fig. 3b**). Finally, the model allowed us to test a much wider range of mean correlated variability values than those collected in our electrophysiological data (**Fig. 2e**).

A general decoding strategy in the face of unpredictable stimuli

We tested the general decoder strategy in the context of a change-detection task because this type of task was used in many of the studies that reported a relationship between perceptual performance and mean correlated variability (Cohen & Maunsell, 2009; 2011; Herrero et al., 2013; Luo & Maunsell, 2015; Mayo & Maunsell, 2016; Nandy et al., 2017; Ni et al., 2018; Ruff & Cohen, 2016; 2019; Verhoef & Maunsell, 2017; Yan et al., 2014; Zénon & Krauzlis, 2012). This simple and well-studied task provided an ideal initial test of our general decoder hypothesis.

However, a general decoding strategy may explain observations in studies that use a variety of behavioral and stimulus conditions. Studies using a variety of tasks have also demonstrated a relationship between perceptual performance and mean correlated variability. These tasks include heading (Gu et al., 2011), orientation (Gregoriou et al., 2014), and contrast (Ruff & Cohen, 2014a; 2014b) discrimination tasks, in which the observer must respond to certain stimulus values or compare stimulus values. Interestingly, some studies of discrimination tasks suggest that the relationship between perceptual performance and mean correlated variability cannot be explained by a specific decoding strategy that maximizes the amount of sensory information extracted for the task (Clery et al., 2017; Gu et al., 2011).

On the other hand, other studies of perceptual performance have found that observers can achieve high levels of perceptual precision under certain circumstances (Burgess et al., 1981; Kersten, 1987). Such studies suggest that decoding strategies that maximize the amount of extracted sensory information might be used in certain situations. Further tests of decoding strategies in a variety of stimulus conditions and behavioral contexts will be necessary to determine when sensory information decoding prioritizes accuracy and when decoding prioritizes flexibility, or generality, over accuracy. Of particular interest is the potential role of perceptual learning (Seitz & Watanabe, 2005) in determining the extent to which decoding is specific (Gu et al., 2011; Jeanne et al., 2013; Ni et al., 2018).

General decoders of all features would be inextricably linked to mean correlated variability

Our results address a paradox in the literature. Electrophysiological and theoretical evidence supports that there is a relationship between mean correlated variability and perceptual performance (Abbott & Dayan, 1999; Clery et al., 2017; Haefner et al., 2013; Jin et al., 2019; Ni et al., 2018; Ruff & Cohen, 2019; reviewed by Ruff et al., 2018). Yet, a specific decoding strategy in which different sets of neuronal weights are used to decode different stimulus changes cannot easily explain this relationship (Kafashan et al., 2021; Kanitscheider et al., 2015b; Moreno-Bote et al., 2014; Pitkow et al., 2015; Rumyantsev et al., 2020; reviewed by Kohn et al., 2016). This is because mean correlated variability is restricted to a small number of dimensions (Ecker et al., 2014; Goris et al., 2014; Huang et al., 2019; Kanashiro et al., 2017; Lin et al., 2015; Rabinowitz et al., 2015; Semedo et al., 2019; Williamson et al., 2016). Specific decoders of neuronal population activity can easily ignore changes along one or few dimensions (Moreno-Bote et al., 2014). In other words, correlated variability changes in one dimension are easy to ignore: observers should simply use one of the many other possible combinations of neuronal responses to guide their perceptual performance.

The general decoder hypothesis offers a resolution to this paradox. As a decoder becomes more general to more stimulus features, its weights will have to depend on more and more tuning properties of the neuronal population. A fully general decoder of stimuli that vary along many feature dimensions would be one whose neuronal weights depend on the tuning properties of the neurons to all stimulus features to which they are selective. For example, two V4 neurons may both prefer vertical orientations. If they also share a color tuning preference for red, a large response from both neurons might indicate vertical orientation, the color red, or a combination of both features. A fully general decoder would need to resolve this discrepancy by choosing weights for these and other neurons that take not only their tuning for orientation but also their tuning for color into account.

Therefore, the weights of a fully general decoder would depend on the tuning of all neurons to all of the stimulus features to which they are selective. A large number of studies have shown that mean correlated variability depends on tuning similarity for all stimulus features (for review, see Cohen & Kohn, 2011; Ruff et al., 2018). The implication is that the decoding weights for a fully general decoder would depend on exactly the same properties as mean correlated variability.

The hypothesis that such a truly general decoder explains the relationship between perceptual performance and mean correlated variability is suggested by our finding that the modeled general decoder for orientation was more strongly related to mean correlated variability than the modeled specific decoder (**Fig. 3d**). However, direct tests of a truly general decoder for multiple stimulus features would be needed to determine if this decoding strategy is used in the face of multiple changing stimulus features. Further, such tests would need to consider alternative hypotheses for how sensory information is decoded when observers observe multiple aspects of a stimulus (Berkes et al., 2009; Deneve, 2012; Lorteije et al., 2015).

In conclusion, the findings of this study support the usefulness of a framework that relates sensory information decoding to behavior (for review, see Panzeri et al., 2017). By first determining the decoder that guided each monkey's behavioral choices, we were able to compare the monkey's decoder to modeled specific and general decoders to test our hypothesis. These results demonstrate that constraining analyses of neuronal data by behavior can provide important insights into the neurobiological mechanisms underlying perception and cognition.

METHODS

Electrophysiological recordings. The subjects were two adult male rhesus monkeys (*Macaca mulatta*, 8 and 10 kg). All animal procedures were approved by the Institutional Animal Care and Use Committees of the University of Pittsburgh and Carnegie Mellon University. Different aspects of these data were presented previously (Ni et al., 2018). We recorded extracellularly from single units and sorted multiunit clusters (the term "unit" refers to either; see Ni et al., 2018) in V4 of the left hemisphere using chronically implanted 96-channel microelectrode arrays (Blackrock Microsystems) with 1 mm long electrodes. We performed all spiking sorting manually using Plexon's Offline Sorter (version 3.3.5, Plexon).

We only included a recorded unit if its stimulus-driven firing rate was both greater than 10 Hz and significantly higher than the baseline firing rate (baseline calculated as the firing rate in the 100 ms window immediately prior to to the onset of the first stimulus per trial; two-sided Wilcoxon signed rank test: $p < 10^{-10}$). The population size of simultaneously recorded units was 8-45 units (mean 39) per day for Monkey 1 and 7-31 units (mean 19) per day for Monkey 2.

Behavioral task. The monkeys performed a change-detection task (**Fig. 1a**; Cohen & Maunsell, 2009) with multiple orientation change options (**Fig. 1b**) and cued attention (Posner, 1980) while we recorded electrophysiological data. We presented visual stimuli on a CRT monitor (calibrated to linearize intensity; 1,024 × 768 pixels; 120 Hz refresh rate) placed 52 cm from the monkey, using custom software written in MATLAB (Psychophysics Toolbox; Brainard, 1997; Pelli, 1997). We monitored each monkey's eye position using an infrared eye tracker (Eyelink 1000; SR Research) and recorded eye position, neuronal responses (30,000 samples/s), and the signal from a photodiode to align neuronal responses to stimulus presentation times (30,000 samples/s) using Ripple hardware.

A trial began when a monkey fixed its gaze on a small, central spot on the video display while two peripheral Gabor stimuli (one overlapping the RFs of the recorded neurons, the other in the opposite visual hemifield; **Fig. 1c**) synchronously flashed on (for 200 ms) and off (for a randomized period between 200-400 ms) at the same starting orientation until at a random, unsignaled time the orientation of one of the stimuli changed. The monkey received a liquid reward for making a saccade to the changed stimulus within 400 ms of its onset.

Attention was cued in blocks of trials, with each block preceded by 10 instruction trials that cued one of the two stimulus locations by only presenting stimuli at that location. Each block consisted of approximately 125 orientation change trials. In each block, the orientation change occurred at the cued location in 80% of the change trials and at the uncued location in 20% of the change trials. Catch trials were intermixed, in which no orientation change occurred within the maximum of 12 stimulus presentations. In catch trials, the monkeys were rewarded for maintaining fixation. Blocks of trials with attention cued to the left hemifield location or to the right hemifield location were presented in alternating order within a recording day.

The changed orientation at the cued location was randomly selected per trial from one of five changed orientations (with the constraint of required numbers of presentations per changed orientation per block; **Fig. 1b**) such that the monkeys could not predict which orientation change amount was to be detected on any given trial. The changed orientation at the uncued location was randomly either the median (20 trials per block) or the largest orientation change amount (5 trials per block). Uncued changes were collected mainly for the median change amount to maximize

the number of uncued trials collected for one change amount. All analyses of the effects of attention analyzed the cued versus uncued median change amounts.

The size, location, and spatial frequency of the Gabor stimuli were fixed across all recording days. These three parameters were determined in advance of recording the data presented here, using a receptive field mapping task. These parameters were set to maximize the neuronal responses recorded by the array.

The starting orientation (**Fig. 1a & b**) was identical for all trials within a day. We changed the starting orientation by 15° for each new day of recording. We also changed the five changed orientation options (**Fig. 1b**) for each new day of recording, to maintain the task at approximately the same level of difficulty across days. The five changed orientation options were always the same within one session of trials, with one session equaling two blocks of trials: one block of trials with the left stimulus cued, and one block of trials with the right stimulus cued (**Fig. 1c**). We sometimes changed the five orientation options between sessions within a day, again to maintain a consistent level of task difficulty. For those days, we binned the orientation change amounts into five bins based on their log distribution.

Electrophysiological data analysis. The data presented are from 46 days of recording for Monkey 1 and 28 days of recording for Monkey 2. Instruction trials were not included in any analyses. Only trials in which the orientation changes occurred at the RF location (**Fig. 1c**) and catch trials were analyzed (see below for specific inclusions per analysis). The first stimulus presentation of each trial was excluded from all analyses to minimize temporal non-stationarities due to adaptation.

Firing rates (**Fig. 2d**), mean correlated variability (**Fig. 2e, 3c**), and covariance eigenspectrum analyses (**Fig. 2f**) were calculated based on orientation change trials on which the monkey correctly detected the change as well as on catch trials. From these trials, only the starting orientation stimulus presentations were included in the analyses. The firing rate per stimulus presentation was based on the spike count response between 60-260 ms after stimulus onset to account for V4 latency. These analyses were performed per recording day (such that all starting orientation stimuli analyzed together were identical). Data were presented as the mean per day (**Fig. 3c**) or across days (**Fig. 2d-f**) per attention condition (cued or uncued).

We defined the mean correlated variability of each pair of simultaneously recorded units (quantified as the noise correlation or spike count correlation; Cohen & Kohn, 2011) as the Pearson's correlation between the firing rates of the two units in response to repeated presentations of the same stimulus (the starting orientation). This measure of mean correlated variability represents correlations in noise rather than in signal because the visual stimulus was always the same.

For **Fig. 3c**, we used Williams' procedure for comparing correlated correlation coefficients (Howell, 2007) to compare the across-days Pearson's correlation between the performance of the monkey's decoder and the mean correlated variability of the V4 population to the across-days Pearson's correlation between the performance of the specific decoder and the mean correlated variability of the V4 population.

For Monkey 1, two outlier points (uncued trials for each of two days) with mean correlated variability values greater than 0.35 were excluded from analysis based on the Tukey method (see **Fig. 3c** for the range of included correlated variability values for Monkey 1). For **Fig. 3c**, with the excluded points included, the Pearson's correlation coefficients were qualitatively unchanged: for the monkey's decoder, n = 88, or 44 days (see below for data

included in decoder analyses) with two attention conditions plotted per day, $r = -0.34$, $p = 1.7 \times 10^{-3}$; for the specific decoder, $r = -0.22$, $p = 0.05$.

V4 population specific decoder. For **Fig. 3a & c**, we calculated the performance of a specific decoder based on the electrophysiologically recorded V4 neuronal population data (Ni et al., 2018). To avoid artifacts in neuronal firing rates due to eye movements in response to the changed orientation, all V4 population decoder analyses were based on neuronal firing rates during an abbreviated time window: 60-130 ms after stimulus onset.

The specific decoder was a linear classifier trained to best differentiate the V4 population responses to the median changed orientation from the V4 responses to the starting orientation presented immediately before it (**Fig. 1d**; first and second principal components shown for illustrative purposes only – analyses were based on neuronal population firing rates). The neuronal weights were calculated per day and per attention condition.

Decoder performance was quantified as the leave-one-out cross-validated proportion of correctly identified orientations (median changed orientation or starting orientation). For **Fig. 3a**, decoder performance was analyzed per number of neurons (*x*-axis). Per neuronal population size, the most responsive neurons (ranked by evoked response: stimulus-evoked firing rate minus baseline firing rate) were analyzed.

For **Fig. 3c**, decoder performance was illustrated for a set number of neurons (Monkey 1: 20 units, Monkey 2: 10 units). The number of neurons analyzed for these plots was selected to maximize the number of included neurons and recording days (Monkey 1: $n = 44$ days, two days with 8 and 19 recorded units excluded; Monkey 2: $n = 27$ days, one day with 7 recorded units excluded).

V4 population monkey's decoder. For **Fig. 3a & c**, we calculated the performance of the monkey's choice decoder as well (**Fig. 1e**). The monkey's decoder was a linear classifier trained on the same set of V4 population responses as the specific decoder described above (the neuronal population firing rates in response to the median changed orientation and in response to the starting orientation presented immediately before it). However, unlike the specific decoder, the monkey's decoder was trained to best differentiate the V4 population responses when the monkey made a saccade indicating it detected the orientation change from the V4 responses when the monkey did not make a saccade (both correctly in response to the starting orientation and incorrectly when the monkey missed the changed orientation).

Decoder performance was quantified just as it was for the specific decoder described above: as the leave-one-out cross-validated proportion of correctly identified orientations (median changed orientation or starting orientation). **Fig. 3a & c** were calculated as described above for the specific decoder.

In summary, the physiological specific and monkey's decoders were trained on different classifications of the same set of V4 responses and thus had different neuronal weights. However, everything else about how they were analyzed was the same, including that their performance was tested on the same task of correctly identifying whether the left-out orientation was the median changed orientation or the starting orientation.

V4 population more-general vs. more-specific decoders. For **Fig. 3f**, we calculated decoders that were increasingly more general, to compare their performance to that of the monkey's decoder. As described above, due to the limited number of behavioral trials collected per day, we could not calculate an ideal general decoder for orientation based on the physiological data as we could based on the modeled data. However, as a sanity check, we wanted to check whether more-general decoders were more strongly related to the monkey's decoder than more-specific decoders. Additionally, we only analyzed trials from the cued attention condition (uncued trials were mainly collected for the median orientation change amount, which is why the median orientation change trials were analyzed in the attention analyses illustrated in **Fig. 3a & c**). As with **Fig. 3c** as described above, decoder performance was illustrated for a set number of neurons (Monkey 1: 20 units, Monkey 2: 10 units).

As above, the monkey's decoder was trained on the median (third; **Fig. 1b**) orientation change trials. The monkey's decoder was trained to best differentiate the V4 population responses when the monkey made a saccade (indicating it detected the orientation change) from the V4 responses when the monkey did not make a saccade. Importantly, we sought to avoid the relationship that would be inherent between the monkey's decoder and any decoder based on those same median (third) orientation change trials. Thus, only the neuronal weights for the monkey's decoder were based on the median (third) orientation change trials. The weights of all of the other decoders in **Fig. 3f** were based on trials other than the median orientation change trials.

The most specific decoder tested in **Fig. 3f** was trained to best differentiate the V4 population responses to the second largest changed orientation from the V4 responses to the starting orientation presented immediately before it. The performance of this specific decoder was quantified as the leave-one-out cross-validated proportion of trials on which the decoder correctly identified whether the left-out orientation was the second largest changed orientation or the starting orientation. The monkey's decoder was then tested on this same task: identifying whether the orientation was the second largest changed orientation or the starting orientation. We calculated the performance of each decoder on each day of recording. We then calculated the across-days Pearson's correlation between the performance of this specific decoder and the performance of the monkey's decoder. The Pearson's correlation coefficient was plotted in the '1 ori' column of **Fig. 3f** for each monkey (n = 2 decoders; 1 per monkey).

We performed this same procedure for increasingly more-general decoders. The decoders illustrated in the '2 oris' column were trained to best differentiate the V4 responses to two changed orientations from the V4 responses to the starting orientation. The two changed orientations used for each '2 oris' decoder were chosen from the four possibilities: the first, second, fourth, and fifth (max) largest changed orientations (n = 12 decoders; 6 per monkey). We calculated the performance of each '2 oris' decoder on the same task as above: identifying whether the orientation was the second largest changed orientation or the starting orientation. Again, we calculated the across-days Pearson's correlation between the performance of each '2 oris' decoder and the performance of the monkey's decoder.

Each '3 oris' decoder was trained to best differentiate the V4 responses to three changed orientations from the V4 responses to the starting orientation (n = 8 decoders; 4 per monkey). The '4 oris' decoder for each monkey was trained to best differentiate the V4 responses to four changed orientations from the V4 responses to the starting orientation (n = 2 decoders; 1 per monkey).

Network model description. The network model is similar to the one in Huang et al. (2019). Briefly, the network consists of three modeled stages: 1) layer (L) 4 neurons of V1, 2) L2/3 neurons of V1, and 3) L2/3 neurons of V4 (**Fig. 2a**). Neurons from each area are arranged on a uniform grid covering a unit square $\Gamma = [-0.5, 0.5] \times [-0.5, 0.5]$. The L4 neurons of V1 are modeled as a population of excitatory neurons, the spikes of which are taken as inhomogeneous Poisson processes with rates determined as below. The L2/3 of V1 and V4 populations are recurrently coupled networks with excitatory and inhibitory neurons. Each neuron is modeled as an exponential integrate-and-fire (EIF) neuron. The connection probability between neurons decays with distance. The network model captures many attention-mediated changes on neuronal responses, such as the reduction of correlated variability within each visual area, increase in correlated variability between visual areas, and the quenching of the low-dimensional correlated variability by attention. The network parameters are the same as those used in Huang et al. (2019) except the following. The feedforward projection width from V1 (L2/3) to V4 is $\alpha^{(3)}_{\text{ffwd}} = 0.05$. The feedforward strength from V1 (L2/3) to V4 is $[J^3_{\text{eF}}, J^3_{\text{iF}}] = \gamma[1, 0.4]$. From the most unattended state to the most attended state (attentional modulation scale from 0 to 1), γ varies from 20 to 23 mV, and the depolarizing current to the inhibitory neurons in V4, μ_i, varies from 0 to 0.5 mV/ms (**Fig. 2**, **Fig. 3b & d**).

The model differs from the previous model (Huang et al., 2019) in the following ways. We modeled the V1 (L4) neurons as orientation selective filters with static nonlinearity and Poisson spike generation (Kanitscheider et al., 2015b). The firing rate of each neuron i is $r_i(\theta, t) = [F_i \times \tilde{I}(\theta, t)]_+$, where F_i is a Gabor filter and $\tilde{I}(\theta, t)$ is a Gabor image corrupted by independent noise following the Ornstein-Uhlenbeck process,

$$\tilde{I}(\theta, t) = I(\theta) + \eta(t) \quad \text{and} \quad \tau_n d\eta_i = -\eta_i dt + \sigma_n dW,$$

with $\tau_n = 40$ ms and $\sigma_n = 3.5$. The Gabor filters were normalized such that the mean firing rate of V1 (L4) neurons was 10 Hz. Spike trains of V1 (L4) neurons were generated as inhomogeneous Poisson processes with rate $r_i(\theta, t)$. The Gabor image is defined on Γ with 25×25 pixels with spatial Gaussian envelope width $\sigma = 0.2$, spatial wavelength $\lambda = 0.6$ and phase $\phi = 0$ (Kanitscheider et al., 2015b, Supp Eq. 6). The Gabor filters of V1 (L4) neurons had the same σ, λ and ϕ as the image (Kanitscheider et al., 2015b, Supp Eq. 5). The orientation θ was normalized between 0 and 1. The orientation preference map of L4 neurons in V1 was generated using the formula from Kaschube et al. (2010, Supp Eq. 20) with average column spacing $\Lambda = 0.2$.

Each network simulation was 20 sec long consisting of alternating OFF (300 ms) and ON (200 ms) intervals. During OFF intervals, spike trains of Layer 1 neurons were independent Poisson processes with rate $r_X = 5$ Hz. An image with a randomly selected orientation was presented during ON intervals. Spike counts during the ON intervals were used to compute the performance of different decoders and correlated variability. The first spike count in each simulation was excluded. For each parameter condition, the connectivity matrices were fixed for all simulations. The initial states of each neuron's membrane potential were randomized in each simulation. All simulations were performed on the CNBC Cluster in the University of Pittsburgh. All simulations were written in a combination of C and Matlab (Matlab R 2015a, Mathworks). The differential equations of the neuron model were solved using the forward Euler method with time step 0.01 ms.

Network model specific decoder. Let $\mathbf{r}$ be a vector of spike counts from all neurons on a single trial, $\mathbf{f}$ be the tuning curve function, and Σ be the covariance matrix. Consider a fine

discrimination task of two orientations $\theta^+ = \theta_0 + d\theta$ and $\theta^- = \theta_0 + d\theta$. The specific decoder is a local linear estimator:

$$\hat{\theta} = \theta_0 + \mathbf{w}^T(\mathbf{r} - \frac{\mathbf{f}(\theta^+) + \mathbf{f}(\theta^-)}{2}).$$

The optimal weight to minimize the mean squared error over all trials, $E = \langle|\hat{\theta} - \theta|^2\rangle$, is

$$\mathbf{w}^s_{\text{opt}} = \frac{\Sigma^{-1}\mathbf{f}'}{\mathbf{f}'\Sigma^{-1}\mathbf{f}'}.$$

The linear Fisher information is equivalent to the inverse of the variance of the optimal specific decoder:

$$I = \frac{1}{\text{Var}(\hat{\theta}_{opt}|\theta^i)} = \mathbf{f}'\Sigma^{-1}\mathbf{f}'.$$

The linear Fisher information is estimated with bias-correction (**Fig. 3b**) (Kanitscheider et al., 2015a):

$$\hat{I} = \frac{(\mathbf{f}^+ - \mathbf{f}^-)^T}{d\theta}\left(\frac{\Sigma^+ + \Sigma^-}{2}\right)^{-1}\frac{(\mathbf{f}^+ - \mathbf{f}^-)}{d\theta}\left(\frac{2N_{\text{tr}} - N - 3}{2N_{\text{tr}} - 2}\right) - \frac{2N}{N_{\text{tr}}d\theta^2}, \tag{1}$$

where $\mathbf{f}^i$ and Σ^i are the empirical mean and covariance, respectively, for θ^i, $i \in \{+, -\}$. The number of neurons sampled is N, and the number of trials for each θ^i is N_{tr}. In simulations, we used $\theta_0 = 0.5$ and $d\theta = 0.01$. There were 58,500 spike counts in total for θ^+ and θ^-.

Network model general decoder. The general decoder is a complex linear estimator $\hat{z} = \mathbf{w^T r}$ (Shamir & Sompolinsky, 2006) where $\mathbf{w}$ is fixed for all θ. The estimator $\hat{z}$ maps the population activity $\mathbf{r}$ in response to all orientations to a circle ($z = e^{i\theta}$ in complex domain). The estimation of orientation is $\hat{\theta} = \arg(\hat{z})$. The optimal weight $\mathbf{w}^g_{\text{opt}}$ that minimizes the mean squared error, $E(\mathbf{w}) = \langle|\hat{z} - z|^2\rangle_{\theta,\mathbf{r}}$, averaged over all θ and trials of $\mathbf{r}$, is

$$\mathbf{w}^g_{\text{opt}} = \langle\Sigma(\theta) + \mathbf{f}\mathbf{f}^T\rangle_\theta^{-1}\langle\mathbf{f}e^{i\theta}\rangle_\theta, \tag{2}$$

The mean squared error of the optimal general decoder is

$$E(\mathbf{w}^g_{\text{opt}}) = 1 - (\langle\mathbf{f}e^{i\theta}\rangle_\theta)^*\langle\Sigma(\theta) + \mathbf{f}\mathbf{f}^T\rangle_\theta^{-1}(\langle\mathbf{f}e^{i\theta}\rangle_\theta),$$

where $*$ denotes the conjugate transpose. Hence, the estimation error of $\hat{z}$ depends on both the covariance matrix, Σ, and tuning similarity, $\mathbf{f}\mathbf{f}^T$. The performance of the general decoder is measured as $I_{\text{g}} = 1/\text{Var}(\hat{\theta})$ (**Fig. 3b**). The estimation of I_{g} is

$$\hat{I}_{\text{g}} = \frac{1}{\text{Var}(\arg((\mathbf{w}^g_{\text{opt}})^T\mathbf{r}) - \theta)}\frac{N_{\text{tr}} - N - 2}{N_{\text{tr}} - 1}, \tag{3}$$

where N_{tr} is the total number of trials for all θ's. In simulations, we used 50 θ's uniformly spaced between 0 and 1. There were 117,000 trials in total for all θ's.

Dependence of network model decoders' performance on correlated variability (Fig. 3d). We trained specific and general decoders on the same spike count dataset ($\mathbf{r}$) in response to pairs of orientations, θ_1 and θ_2 (with difference $\Delta\theta = 0.04$). The specific decoder was trained on the N-dimensional space of neural responses, using support vector machine model with two-fold cross-validation to linearly classify $\mathbf{r}$ for the two orientations. The general decoder first maps $\mathbf{r}$ to a two-dimensional plane $\hat{z} = (\mathbf{w}^g_{\text{opt}})^T\mathbf{r}$ using the optimal weight $\mathbf{w}^g_{\text{opt}}$ (**Eq. 2**) computed with the spike counts of all orientations. Then a two-dimensional support vector machine model with two-fold cross-validation was trained to linearly classify $\hat{z}$ for θ_1 and θ_2. The correlated variability was computed from the spike counts data for θ_1 of each pair. There were 200 sampling of $N = 100$ excitatory neurons from the V4 network, and 10 orientation pairs varying between 0 and 1. There were on average 2,340 trials for each θ.

Factor analysis for network model. Let $x \in \mathbb{R}^{n\times 1}$ be the spike counts from n simultaneously recorded neurons. Factor analysis assumes that x is a multi-variable Gaussian process:

$$x \sim \mathcal{N}(\mu, LL^T + \Psi)$$

where $\mu \in \mathbb{R}^{n\times 1}$ is the mean spike counts, $L \in \mathbb{R}^{n\times m}$ is the loading matrix of the m latent variables and $\Psi \in \mathbb{R}^{n\times 1}$ is a diagonal matrix of independent variances for each neuron (Cunningham & Yu, 2014). We chose $m = 5$ and compute the eigenvalues of LL^T, λ_i $(i = 1, 2, \ldots, m)$, ranked in descending order. Spike counts were collected using 200 ms window. There were on average 2,340 trials per attentional condition.

Data availability. Electrophysiological data analyzed in this manuscript are available at https://pitt.box.com/v/NiRuffAlbertsSymmondsCohen2017.

Code availability. Computer code for all simulations and analysis of the resulting data will be available at https://github.com/hcc11/.

Acknowledgements. A.M.N. is supported by US NIH grant 1K99NS118117-01 and a fellowship from the Simons Foundation Collaboration on the Global Brain. C.H. is supported by a Swartz Foundation Fellowship #2017-7 and a grant from the Simons Foundation Collaboration on the Global Brain. B.D. is supported by US NIH grants 1U19NS107613-01 and R01EB026953, a Vannevar Bush faculty fellowship N00014-18-1-2002, and a grant from the Simons Foundation Collaboration on the Global Brain. M.R.C. is supported by US NIH grants 4R00EY020844-03, R01 EY022930, and Core Grant P30 EY008098s, a grant from the Whitehall Foundation, a Klingenstein-Simons Fellowship, a Sloan Research Fellowship, a McKnight Scholar Award, and a grant from the Simons Foundation Collaboration on the Global Brain. We thank Douglas A. Ruff, Joshua J. Alberts, and Jen Symmonds for assistance with data collection. We thank Karen McCracken for technical assistance. We thank Alexandre Pouget and Douglas A. Ruff for comments on a previous version of the manuscript.

Competing interests. The authors declare no competing financial interests.

Author contributions. A.M.N., C.H., B.D., and M.R.C. designed the project; A.M.N. collected and analyzed the electrophysiological data; C.H. performed the model simulations and analyzed the model data; M.R.C. supervised the project; A.M.N., C.H., B.D., and M.R.C. contributed to writing the manuscript.

REFERENCES

Abbott, L. F. & Dayan, P. The effect of correlated variability on the accuracy of a population code. *Neural Comput* .**11,** 91-101 (1999).

Berkes, P., Turner, R. E. & Sahani, M. A structured model of video reproduces primary visual cortical organisation. *PLoS Comput. Biol.* **5**, e1000495 (2009).

Brainard, D. H. The Psychophysics Toolbox. *Spat. Vis.* **10,** 433-436 (1997).

Burgess, A. E., Wagner, R. F., Jennings, R. J. & Barlow, H. B. Efficiency of human visual signal discrimination. *Science* **214**, 93-94 (1981).

Clery, S., Cumming, B. G. & Nienborg, H. Decision-Related Activity in Macaque V2 for Fine Disparity Discrimination Is Not Compatible with Optimal Linear Readout. *J. Neurosci.* **37,** 715-725 (2017).

Cohen, M. R. & Kohn, A. Measuring and interpreting neuronal correlations. *Nat. Neurosci.* **14,** 811-819 (2011).

Cohen, M. R. & Maunsell, J. H. R. Attention improves performance primarily by reducing interneuronal correlations. *Nat. Neurosci.* **12,** 1594-1600 (2009).

Cohen, M. R. & Maunsell, J. H. R. Using neuronal populations to study the mechanisms underlying spatial and feature attention. *Neuron* **70,** 1192-1204 (2011).

Cunningham, J. P. & Yu, B. M. Dimensionality reduction for large-scale neural recordings. *Nat. Neurosci.* **17,** 1500-1509 (2014).

Deneve, S. Making decisions with unknown sensory reliability. *Front. Neurosci.* **6**, 75 (2012).

Ecker, A. S., Berens, P., Cotton, R. J., Subramaniyan, M., Denfield, G. H., Cadwell, C. R., Smirnakis, S. M., Bethge, M. & Tolias, A. S. State dependence of noise correlations in macaque primary visual cortex. *Neuron* **82,** 235-248 (2014).

Goris, R. L., Movshon, J. A. & Simoncelli, E. P. Partitioning neuronal variability. *Nat. Neurosci.* **17,** 858-865 (2014).

Gregoriou, G. G., Rossi, A. F., Ungerleider, L. G. & Desimone, R. Lesions of prefrontal cortex reduce attentional modulation of neuronal responses and synchrony in V4. *Nat. Neurosci.* **17,** 1003-1011 (2014).

Gu, Y., Liu, S., Fetsch, C. R., Yang, Y., Fok, S., Sunkara, A., DeAngelis, G. C. & Angelaki, D. E. Perceptual learning reduces interneuronal correlations in macaque visual cortex. *Neuron* **71,** 750-761 (2011).

Haefner, R. M., Gerwinn, S., Macke, J. H. & Bethge, M. Inferring decoding strategies from choice probabilities in the presence of correlated variability. *Nat. Neurosci.* **16**, 235-242 (2013).

Herrero, J. L., Gieselmann, M. A., Sanayei, M. & Thiele, A. Attention-induced variance and noise correlation reduction in macaque V1 is mediated by NMDA receptors. *Neuron* **78,** 729-739 (2013).

Howell, D. C. *Statistical Methods for Psychology* (Thomson Wadsworth, Belmont, CA, 2007).

Huang, C., Pouget, A. & Doiron, B. Internally generated population activity in cortical networks hinders information transmission. *bioRxiv* doi: 10.1101/2020.02.03.932723 (2020).

Huang, C., Ruff, D. A., Pyle, R., Rosenbaum, R., Cohen, M. R. & Doiron, B. Circuit Models of Low-Dimensional Shared Variability in Cortical Networks. *Neuron* **101,** 337-348 e334 (2019).

Jeanne, J. M., Sharpee, T. O. & Gentner, T. Q. Associative learning enhances population coding by inverting interneuronal correlation patterns. *Neuron* **78**, 352-363 (2013).

Jin, M., Beck, J. M. & Glickfeld, L. L. Neuronal Adaptation Reveals a Suboptimal Decoding of Orientation Tuned Populations in the Mouse Visual Cortex. *J. Neurosci.* **39,** 3867-3881 (2019).

Kafashan, M., Jaffe, A. W., Chettih, S. N., Nogueira, R., Arandia-Romero, I., Harvey, C. D., Moreno-Bote, R. & Drugowitsch, J. Scaling of sensory information in large neural populations shows signatures of information-limiting correlations. *Nat. Commun.* **12**, 473 (2021).

Kanashiro, T., Ocker, G. K., Cohen, M. R. & Doiron, B. Attentional modulation of neuronal variability in circuit models of cortex. *Elife* **6,** e23978 (2017).

Kanitscheider, I., Coen-Cagli, R., Kohn, A. & Pouget, A. Measuring Fisher information accurately in correlated neural populations. *PLoS Comput. Biol.* **11,** e1004218 (2015a).

Kanitscheider, I., Coen-Cagli, R. & Pouget, A. Origin of information-limiting noise correlations. *Proc. Natl. Acad. Sci. U S A* **112,** E6973-E6982 (2015b).

Kaschube, M., Schnabel, M., Lowel, S., Coppola, D. M., White, L. E. & Wolf, F. Universality in the evolution of orientation columns in the visual cortex. *Science* **330,** 1113-1116 (2010).

Kersten, D. Statistical efficiency for the detection of visual noise. *Vision Res.* **27**, 1029-1040 (1987).

Kohn, A., Coen-Cagli, R., Kanitscheider, I. & Pouget, A. Correlations and Neuronal Population Information. *Annu. Rev. Neurosci*. **39,** 237-256 (2016).

Lin, I. C., Okun, M., Carandini, M. & Harris, K. D. The Nature of Shared Cortical Variability. *Neuron* **87,** 644-656 (2015).

Lorteije, J. A. M., Zylberberg, A., Ouellette, B. G., De Zeeuw, C. I., Sigman, M. & Roelfsema, P. R. The Formation of Hierarchical Decisions in the Visual Cortex. *Neuron* **87**, 1344-1356 (2015).

Luo, T. Z. & Maunsell, J. H. R. Neuronal Modulations in Visual Cortex Are Associated with Only One of Multiple Components of Attention. *Neuron* **86,** 1182-1188 (2015).

Mayo, J. P. & Maunsell, J. H. R. Graded Neuronal Modulations Related to Visual Spatial Attention. *J. Neurosci.* **36,** 5353-5361 (2016).

Mitchell, J. F., Sundberg, K. A. & Reynolds, J. H. Spatial attention decorrelates intrinsic activity fluctuations in macaque area V4. *Neuron* **63,** 879-888 (2009).

Moreno-Bote, R., Beck, J., Kanitscheider, I., Pitkow, X., Latham, P. & Pouget, A. Information-limiting correlations. *Nat. Neurosci.* **17,** 1410-1417 (2014).

Nandy, A. S., Nassi, J. J. & Reynolds, J. H. Laminar Organization of Attentional Modulation in Macaque Visual Area V4. *Neuron* **93,** 235-246 (2017).

Ni, A. M., Ruff, D. A., Alberts, J. J., Symmonds, J. & Cohen, M. R. Learning and attention reveal a general relationship between population activity and behavior. *Science* **359,** 463-465 (2018).

Nirenberg, S. & Latham, P. E. Decoding neuronal spike trains: how important are correlations? *Proc. Natl. Acad. Sci. U S A* **100**, 7348-7353 (2003).

Panzeri, S., Harvey, C. D., Piasini, E., Latham, P. E. & Fellin, T. Cracking the neural code for sensory perception by combining statistics, intervention, and behavior. *Neuron* **93**, 491-507 (2017).

Pelli, D. G. The VideoToolbox software for visual psychophysics: transforming numbers into movies. *Spat. Vis.* **10,** 437-442 (1997).

Pitkow, X., Liu, S., Angelaki, D. E., DeAngelis, G. C. & Pouget, A. How Can Single Sensory Neurons Predict Behavior? *Neuron* **87**, 411-423 (2015).

Posner, M. I. Orienting of attention. *Q. J. Exp. Psychol.* **32,** 3-25 (1980).

Rabinowitz, N. C., Goris, R. L., Cohen, M. & Simoncelli, E. P. Attention stabilizes the shared gain of V4 populations. *Elife* **4,** e08998 (2015).

Ruff, D. A. & Cohen, M. R. Attention can either increase or decrease spike count correlations in visual cortex. *Nat. Neurosci.* **17,** 1591-1597 (2014a).

Ruff, D. A. & Cohen, M. R. Global cognitive factors modulate correlated response variability between V4 neurons. *J. Neurosci.* **34,** 16408-16416 (2014b).

Ruff, D. A. & Cohen, M. R. Stimulus Dependence of Correlated Variability across Cortical Areas. *J. Neurosci.* **36,** 7546-7556 (2016).

Ruff, D. A. & Cohen, M. R. Simultaneous multi-area recordings suggest that attention improves performance by reshaping stimulus representations. *Nat. Neurosci.* **22**, 1669-1676 (2019).

Ruff, D. A., Ni, A. M. & Cohen, M. R. Cognition as a Window into Neuronal Population Space. *Annu. Rev. Neurosci.* **41**, 77-97 (2018).

Rumyantsev, O. I., Lecoq, J. A., Hernandez, O., Zhang, Y., Savall, J., Chrapkiewicz, R., Li, J., Zeng, H., Ganguli, S. & Schnitzer, M. J. Fundamental bounds on the fidelity of sensory cortical coding. *Nature*, **580**, 100-105 (2020).

Seitz, A. & Watanabe, T. A unified model for perceptual learning. *Trends Cogn. Sci.* **9**, 329-334 (2005).

Semedo, J. D., Zandvakili, A., Machens, C. K., Yu, B. M. & Kohn, A. Cortical Areas Interact through a Communication Subspace. *Neuron* **102,** 249-259 e244 (2019).

Shamir, M. & Sompolinsky, H. Implications of neuronal diversity on population coding. *Neural Comput.* **18,** 1951-1986 (2006).

Verhoef, B. E. & Maunsell, J. H. R. Attention-related changes in correlated neuronal activity arise from normalization mechanisms. *Nat. Neurosci.* **20,** 969-977 (2017).

Williamson, R. C., Cowley, B. R., Litwin-Kumar, A., Doiron, B., Kohn, A., Smith, M. A. & Yu, B. M. Scaling Properties of Dimensionality Reduction for Neural Populations and Network Models. *PLoS Comput. Biol.* **12,** e1005141 (2016).

Yan, Y., Rasch, M. J., Chen, M., Xiang, X., Huang, M., Wu, S. & Li, W. Perceptual training continuously refines neuronal population codes in primary visual cortex. *Nat. Neurosci.* **17,** 1380-1387 (2014).

Zénon, A. & Krauzlis, R. J. Attention deficits without cortical neuronal deficits. *Nature* **489,** 434-437 (2012).